ELSEVIER

Journal of Nuclear Materials 241–243 (1997) 414–419

journal of nuclear materials

Measurement and analysis of radiated power components in the JET MkI divertor using VUV spectroscopy

C.F. Maggi [a,*], J.D. Elder [a,b], W. Fundamenski [a,b], R. Giannella [a], L.D. Horton [a], K.D. Lawson [a,c], A. Loarte [a], A. Maas [a], R. Reichle [a], M. Stamp [a], P.C. Stangeby [a,b], H.P. Summers [a,d]

[a] *JET Joint Undertaking, Abingdon, Oxon OX14 3EA, UK*
[b] *Institute for Aerospace Studies, University of Toronto, Toronto, Ontario, Canada M3H 5T6*
[c] *UKAEA Government Division, Fusion, Culham, Oxon OX14 3DB, UK*
[d] *University of Strathclyde, Glasgow, G4 ONG, UK*

Abstract

This paper presents a spectroscopic study of deuterium and impurity radiation in the MkI divertor of JET in different experimental regimes. Radiated power measurements using absolutely calibrated VUV spectroscopy are consistent with bolometer measurements in a variety of impurity scenarios. These observations, combined with measurements of visible emission, are compared with code predictions of divertor radiation distributions, highlighting uncertainties in the description of the background plasma and of the carbon source, which affect detailed modelling of divertor impurity transport.

Keywords: JET; Divertor plasma; Radiation diagnostic; Impurity transport

1. Introduction

When modelling hydrogenic and impurity emission from the divertor the overall experimental features can be well reproduced, especially in low density regimes. On the other hand, the understanding of the transport mechanisms that determine the specific radiation profiles, both in terms of spatial distributions and of ionization balance, is far from complete, especially in high density and plasma detachment regimes [1]. A further complication is due to the large uncertainties associated with modelling of the impurity source, as exemplified by carbon in this study. Simultaneous spectroscopic observations of divertor plasma emission, both in the VUV and visible region, provide essential information in this area of study. In this paper spectroscopic measurements from the JET divertor and their comparison with interpretative code modelling are presented.

* Corresponding author. Tel.: +44-1235 465335; fax: +44-1235 464535; e-mail: cfm@jet.uk.

2. Intrinsic impurities

2.1. Spectroscopic observations

VUV line emission was measured at JET by an absolutely calibrated double SPRED spectrometer along a vertical line of sight (LOS) directed at the inner target of the MkI divertor. The double SPRED spans simultaneously a wavelength range of 150–1450 Å. The spectrometers were calibrated in situ by means of branching ratio techniques, using a visible LOS through the central bore of the VUV system. The uncertainty in the absolute calibration is 50%. The radiated power measured by VUV spectroscopy in different impurity scenarios and plasma regimes is consistent with that measured with a bolometer with a view similar to that of the double SPRED. This view, which traverses the X-point region, also corresponds to that of maximum radiation at high density.

In the absence of impurity injection, emission from D I and C II–IV dominates in the divertor in Ohmic, L-mode and H-mode discharges at moderate to high densities. The deuterium radiated power is measured spectroscopically

PII S0022-3115(96)00539-9

from L_α and L_β. The C II–III radiated power is measured from the resonance transitions, while the C IV line power has the largest uncertainty, since the C IV resonance line is not measured and the power is calculated from line ratios of the measured $n = 3$–$n = 2$ transitions (which depend weakly on the electron temperature) using a collisional radiative model [2]. From this analysis C III is the strongest radiator of the carbon ionization stages. Radiated power components measured by VUV spectroscopy are shown in Fig. 1 for an Ohmic discharge in which the density was ramped, by means of deuterium gas fuelling in the divertor, from 2.0 to 5.6×10^{19} m^{-3}, when the density limit occurred (not shown in the figure). The spectroscopic signals are more strongly influenced by the strike point sweeping across the target, due to the narrower acceptance cone of the VUV spectrometer. When comparing with spectroscopy, the core contribution is subtracted from the bolometer measurement using a near-horizontal bolometer view and assuming uniform emission inside the last closed magnetic flux surface. Radiation from C I was not measured and was estimated to be negligible, consistent with simulations. The resonance transitions of C V–VI were not measured, but from the Balmer$_\alpha$ transition in C VI and the $n = 3$–$n = 2$ transitions in C V it was estimated, over a range of divertor-relevant electron densities and temperatures, that emission from these ionization stages did not contribute significantly to the power balance, as confirmed by the simulations.

These results apply to discharges operated both on carbon and beryllium divertor targets, suggesting that during beryllium operation the target surfaces were coated with a carbon layer, possibly originating from sputtering at the carbon walls of the JET tokamak. This observation shows why characteristics of plasmas on beryllium and carbon targets were similar [3].

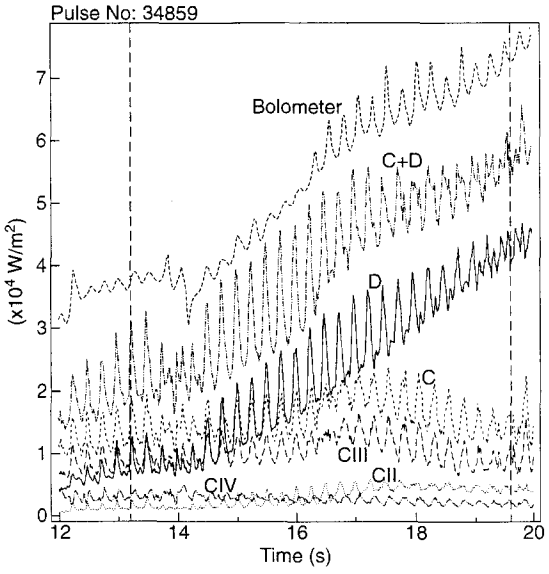

Fig. 1. Bolometer and VUV spectroscopy radiated power measurements for an Ohmic density limit discharge on Be target. The vertical dashed lines mark the time slices chosen for comparison with modelling.

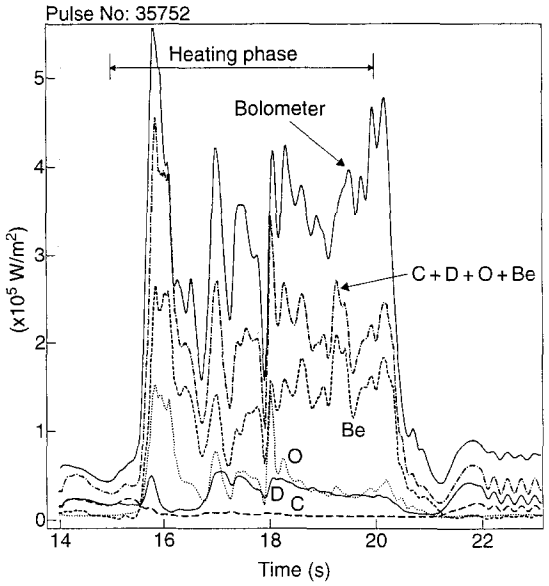

Fig. 2. Radiated power components measured by VUV spectroscopy during a discharge with Be target melting.

A series of experiments was carried out in the final period of the MkI divertor campaign to assess plasma performance on molten beryllium divertor target plates [4]. Fig. 2 shows VUV emission measured during one such discharge, when about 15 MW of additional heating was applied without sweeping of the strike points. During this phase beryllium is the strongest radiator, with Be II carrying most of the power towards the end of the heating phase. At the same time, the carbon line radiation is observed to decrease by an order of magnitude. Radiated power components for Be II are derived from $n = 4$–$n = 2$ transitions and for Be III–IV from $n = 3$–$n = 2$ transitions with collisional radiative calculations [2]. The lack of measurements of resonance line emission leads to large uncertainties (a factor of 2 or more) in the evaluated beryllium radiation. As the power load to the target is increased and melting occurs, oxygen is released (Fig. 2), most likely following molecular breakup of beryllium oxides. The oxygen radiation level, measured from the resonance transitions of O III–VI, returns to negligible levels when the targets cool after the additional heating is switched off. Of the oxygen ionization stages, O VI is the strongest radiator.

2.2. Comparison with code simulations

The Ohmic discharge shown in Fig. 1 was modelled in the low density and plasma detachment phases using 2D

Monte Carlo simulations (DIVIMP [5]/NIMBUS [6]) of impurity and neutral hydrogen transport. These simulations are used to interpret the spectroscopic measurements in the divertor environment and, in turn, the physics assumptions in the models are questioned by the experimental findings.

In the low density phase of the discharge, the hydrogenic background plasma is obtained by solving the steady state fluid equations for classical transport along the magnetic field, with boundary conditions from Langmuir probe measurements of n_e, T_e at the divertor target ('onion skin' model within DIVIMP [7]). The target ion temperature is not measured and is therefore assumed equal to the electron temperature. A converged plasma solution is reached by iterating with NIMBUS, thus obtaining the hydrogen ionization source distribution, as well as the neutral carbon ionization distribution. Physical and chemical sputtering from the background plasma and impurity self-sputtering determine the carbon source. Carbon production due to physical sputtering is obtained using the revised Bohdansky formula, with data as in [8]. The chemical yields are taken from the measured CD_4 yields as in [9]. Chemical sputtering is then modelled by releasing 0.1 eV carbon atoms from the target/wall surfaces. A constant $D_\perp = 1$ m^2/s for all impurity ionization stages is assumed. Physical sputtering only accounts for the beryllium source, but BeO has to be assumed as target material in the model to reproduce Be II emission, measured by a flux camera viewing the divertor region from the top of the machine (Fig. 3a). This has the effect of both lowering the sputtering yield and increasing the threshold energy for sputtering with respect to the case of pure beryllium. This choice is

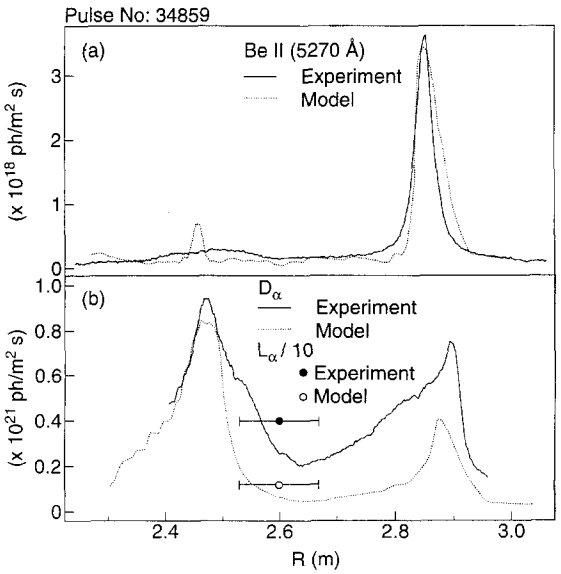

Fig. 3. Experimental and simulated Be II (a) and D_α (b) emission at low density for the Ohmic pulse of Fig. 2. Also shown is the comparison for L_α emission along the VUV spectrometer view.

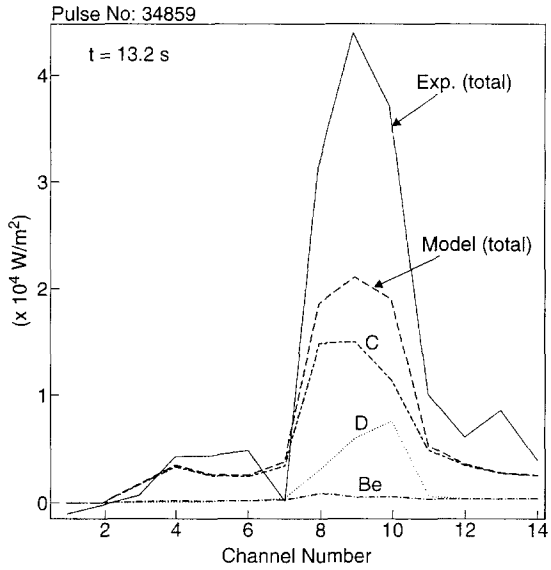

Fig. 4. Experimental and simulated bolometer radiated power at low density for pulse 34859.

also supported by the spectroscopic observations during beryllium target melting experiments, reported earlier, showing that under normal operation oxygen is gettered by beryllium. In principle, a more realistic picture would have been to include in the model the effect of carbon contamination of the beryllium target surfaces, but sputtering yields for beryllium carbides are not available.

The simulated beryllium radiation (Fig. 4) is negligible (< 1 kW/m^2) as expected from the spectroscopic observations. The total radiated power is a factor of two lower than that measured with the bolometer. This discrepancy is mostly due to underestimation of the deuterium radiation, especially in the private flux region (Fig. 3b). The reason for this is still unclear, although neutral recirculation in the subdivertor region is thought to play a role [1]. The total carbon radiation is in agreement with the VUV measurements (Figs. 1 and 4), but the ratio of C III to C IV radiation is underestimated by a factor of five with respect to the experimental value. This is attributed to incorrect modelling of the carbon source from the private plasma target due to the incorrect description of the deuterium density in this region. In fact the VUV spectrometer LOS, which does not view the strike points, is particularly sensitive to carbon sputtering yields in the private plasma. Instead, C II–IV visible spectroscopy measurements integrated over the entire emission profiles are well reproduced.

In the detached phase of the discharge, the background plasma is prescribed both in the SOL and private flux region, so as to reproduce the measured bremsstrahlung and D_α emission profiles from the divertor. In the SOL the hydrogenic plasma is prescribed according to a 3-zone (collision, radiation, conduction) detachment model, which

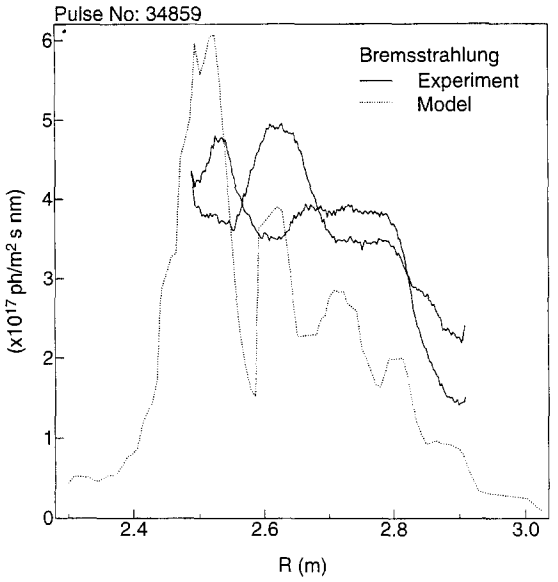

Fig. 5. Experimental and simulated bremsstrahlung emission at detachment for pulse 34859. Two experimental profiles, within one cycle of the strike point sweeping, approximate the full profile measured by the flux camera.

is an extension of the model proposed in [10]. In the collision zone the solution starts with Langmuir probe measurements of n_e, T_e at the targets. The density is then raised a factor of 10 some distance along the field lines, while the temperature is kept constant. In the radiation zone the solution is obtained according to power balance, with specified radiated power fraction with respect to the power flow to the divertor target. In the conduction zone the fluid equations are solved. A 10 eV MARFE is also prescribed in the core at the X-point, to reproduce the measured bremsstrahlung emission (Fig. 5), specifying the values of the temperature on each flux tube in the core at the location on that tube nearest to the X-point. The density is adjusted to give pressure balance along the flux tubes and to match the midplane value. The private plasma is prescribed independently, starting from Langmuir probe measurements at the target and increasing n_e along the field, while T_e is kept constant.

The simulated deuterium radiated power is in agreement with the VUV measurements and 90% of the total D_α emission is due to recombination. The carbon source, which is mainly due to chemical sputtering, is overestimated by the model by a factor of 10 and thus the chemical yield has to be reduced to 0.5% in order to obtain overall agreement with C II visible emission integrated over the inner and outer divertor target region. It is possible that this large discrepancy is due to considerably reduced CD_4 fuelling efficiencies at high deuterium fluxes to the divertor targets, as already reported in other machines, such as AUG [11]. In the simulation, the ratio of C III to C IV radiation (0.3) is inconsistent with the VUV measurements (5.0). This is thought to be due in part to underestimation of the carbon source in the private flux region and to a greater extent to the effect of the temperature-gradient force driving the impurities away from the X-point in the SOL towards higher temperature regions where C IV radiation dominates. DIVIMP simulations of a similar discharge using an EDGE2D/NIMBUS [12] self-consistent background plasma solution produce a higher value of C III/C IV radiation (0.7), which is still much smaller than the experimental one. In this solution the impurity radiation is well concentrated in a region close to the X-point, indicating the presence of a strong neutral friction force which equilibrates the thermal force on the impurities.

3. Effect of change in the divertor flux expansion on C versus D radiation

The effect of plasma-wall clearance on the relative importance of carbon and deuterium radiation is studied for a series of Ohmic density limit discharges with deuterium gas fuelling in the divertor. All these discharges were very similar but are distinguished in two sets by the difference in the divertor flux expansion. For all of the discharges the ratio of carbon to deuterium radiation, measured by VUV spectroscopy, progressively decreases with increasing plasma density and radiated power fraction, P_{RAD}/P_{IN}. However, in the case of high plasma

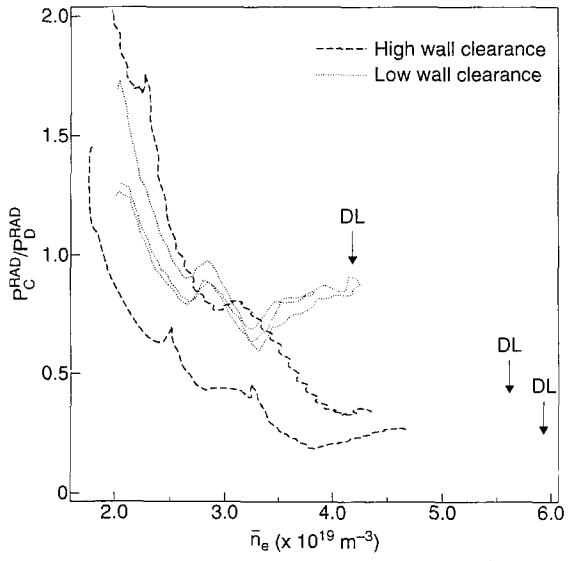

Fig. 6. Ratio of carbon to deuterium radiated power versus volume averaged density for low flux expansion (#34859, #34530) and high flux expansion (#34855, #34856, #34866) discharges. Also shown is the density at the occurrence of the density limit (DL).

clearance from the vertical walls (i.e. low flux expansion in the divertor), deuterium radiation strongly dominates at high density, whereas at low wall clearance (i.e. high flux expansion) the radiated power is equally distributed between deuterium and carbon (Fig. 6), presumably due to increased impurity influx from the walls. These observations are correlated with the occurrence of the density limit at higher densities for discharges with high wall clearance, though $P_{RAD}/P_{IN} \sim 80\%$ for both high and low wall clearance cases at the density limit.

4. Nitrogen seeded radiative divertor

Radiative divertor discharges have been studied in JET during the MkI divertor phase by means of combined nitrogen seeding and deuterium fuelling in the divertor chamber [13]. As the plasma density increases, the peakedness of the X-point radiation increases and at detachment tomographic reconstructions show the radiation peak to occur above the X-point [14]. The nitrogen radiation was measured spectroscopically from line emission of the resonance transitions of N II–V, Li-like nitrogen being the strongest radiator.

The detached phase of a nitrogen radiative divertor discharge was modelled, following trace nitrogen particles (DIVIMP) on a self-consistent, 2D multi-fluid background plasma solution obtained with EDGE2D as reported in [1]. At the time chosen for the simulation this discharge was characterized by 11 MW of total input power, with nitrogen gas rate of 3×10^{22} electrons/s, deuterium gas rate of 1×10^{22} electrons/s and volume averaged density of 4×10^{19} m^{-3}. The total radiated power was 8 MW, with about

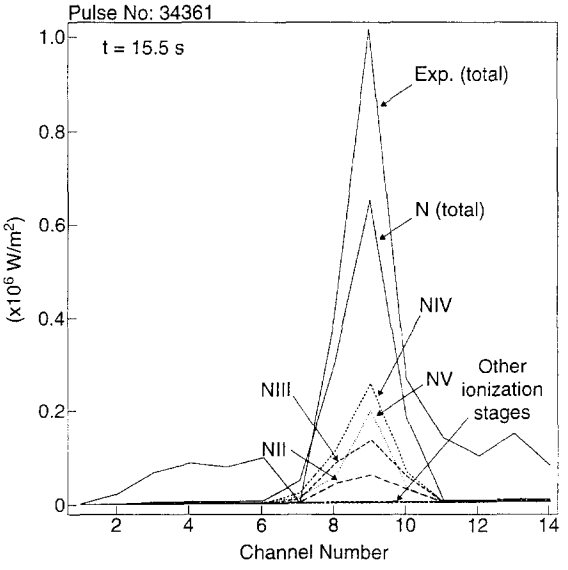

Fig. 7. Experimental (total) and simulated (nitrogen) bolometer radiated power at detachment for a radiative divertor discharge with combined nitrogen seeding and deuterium fuelling in the divertor.

6 MW radiated in the X-point/divertor region. The nitrogen radiation, measured by VUV spectroscopy, was about 80% of the total power measured by the bolometer at detachment, while the remaining 20% was observed to be radiated by carbon and deuterium.

Since in the simulation nitrogen is treated as recycling impurity, the nitrogen source has to be normalized with respect to the experiment. This is obtained by normalizing the calculated radiated power to the power radiated in the X-point/divertor region as measured by the bolometer. However, the calculated Z_{eff} is a factor of three lower than the experimental one, measured by visible bremsstrahlung. A similar discrepancy for Z_{eff} is found when simulating the same discharge with EDGE2D/NIMBUS [1], but the reason of this is still unclear. The comparison between experimental and simulated bolometer radiated power at detachment is shown in Fig. 7. The calculated radiation profile is in good agreement with the experimental one, but the measured ratio of N V to N IV radiated power (3.0) is not reproduced in the simulation, which weights the radiation distribution around N IV. This is thought to be due to underestimation of the electron temperature in the divertor region, thus suppressing the contribution from Li-like nitrogen radiation.

5. Conclusions

Absolutely calibrated VUV measurements of deuterium and impurity line emission in the JET MkI divertor have been presented. They provide essential information towards improved understanding of hydrogenic and impurity transport and production mechanisms in the divertor region.

In the absence of impurity injection, carbon and deuterium account for the total radiated power in diverted discharges on both carbon and beryllium target plates, consistent with simulations. This suggests that the beryllium targets were coated with carbon sputtered from the walls of the tokamak. In medium/high density divertor discharges C III is found to be the strongest radiator of the carbon ionization stages. More work is in progress to ascertain if this is due to modifications of the carbon equilibrium power function due to transport in the divertor or to the lack of measurement of the C IV resonance line. The measured beryllium emission is reproduced in the model if physical sputtering from BeO target surfaces is assumed. Beryllium radiation dominates only during beryllium target melting experiments, when significant additional heating is applied without sweeping of the strike points. In Ohmic density limit discharges the ratio of carbon to deuterium radiation is observed to vary by a factor of two at high density, when varying the divertor flux expansion. This can be explained by the relative importance of sputtering from the divertor sidewalls and has a significant effect on the density limit.

Discrepancies in the detail of the radiation distributions

between measurements and simulations are attributable to underestimation of the carbon source in the private plasma region. This is caused by inadequate modelling of the neutral deuterium density in the private plasma. These discrepancies are accentuated at detachment by the difficulty in describing the impurity forces which can produce the radiation profiles observed experimentally. Further work is needed in order to understand the transport mechanisms connecting the impurity sources and the radiation distributions measured spectroscopically.

References

[1] A. Loarte, these Proceedings, p. 118.
[2] H.P. Summers, ADAS, JET-IR(94) 06 (1994).
[3] D.J. Campbell et al., these Proceedings, p. 379.
[4] B.J.D. Tubbing et al., Plasma Phys. Control. Fusion, Proc. 22nd EPS Conf. (1995) III-453.
[5] P.C. Stangeby and J.D. Elder, J. Nucl. Mater. 196–198 (1992) 258.
[6] E. Cupini, A. De Matteis and R. Simonini, NET Report EUR XII (1984) 324/9.
[7] P.C Stangeby et al., these Proceedings, p. 358.
[8] W. Eckstein et al., IPP Report, IPP-9/82 (1993).
[9] A. Pospieszczyk et al., Plasma Phys. Control. Fusion, Proc. 22nd EPS Conf. (1995) II-309.
[10] K. Borras and P.C. Stangeby, Plasma Phys. Control. Fusion, Proc. 20th EPS Conf. (1993) II-763.
[11] A. Kallenbach et al., Nucl. Fusion 34 (1994) 1557.
[12] R. Simonini et al., Contrib. Plasma Phys. 34 (1994) 368.
[13] G.F. Matthews, Plasma Phys. Control. Fusion 37 (1995) A227.
[14] R. Reichle et al., Plasma Phys. Control. Fusion, Proc. 22nd EPS Conf. (1995) III-85.